Design and direct optimization of spatially fed metasurfaces: software defined highly shaped coverage Reflectarray antenna

Andrea Guarriello, Daniele Bresciani, Renaud Loison, Hervé Legay

Design and direct optimization of spatially fed metasurfaces: software defined highly shaped coverage Reflectarray antenna

Andrea Guarriello[1], Daniele Bresciani[2], Renaud Loison[1], Herve Legay[2]
[1]IETR, National Institute of Applied Sciences, Rennes, France, andrea.guarriello|renaud.loison@insa-rennes.fr
[2]Thales Alenia Space, France, daniele.bresciani|herve.legay@thalesaleniaspace.com.

***Abstract*—As a result of a decade-long collaboration between Thales Alenia Space and IETR (Institut d'Electronique et des Technologies du numéRique) through their joint laboratory, Merlin, a versatile tool for designing and optimizing spatially fed metasurfaces has been developed. This tool, known as DOMES (Direct Optimization of MEtaSurface), is a multi-modular system that integrates modified physical optics and periodic surface analysis tools from Thales Alenia Space, along with advancements in unit cell design and optimization from various research projects conducted within the Merlin framework.**

DOMES employs a general methodology to enhance the efficiency of direct optimization for radiated co-polarization and cross-polarization in large aperture antennas composed of quasi-periodic reflective surfaces (QPRS). It achieves this by ensuring layout continuity without abrupt geometrical variations. This is accomplished through the utilization of the properties of Phoenix cells (PC), efficient parametrization and interpolation of PC databases, and the description of QPRS using continuous B-spline functions. This approach reduces the dimensions of the large-scale optimization problem and naturally ensures smoothness in the layout.

The purpose of this work is to illustrate the general principles of the design and optimization tool, with a focus on two applications involving highly shaped coverage for large deployable Reflectarray (RA) antennas. Each of these use cases involves a problem at a large to very-large electrical size scale. The performance of the RA antennas is compared to equivalent theoretically shaped reflectors, demonstrating that RAs can be highly competitive or even superior in terms of performance.

I. Introduction

Designing and optimizing contoured beam reflectarrays (RAs) for high-gain antenna applications is a complex process with numerous design parameters. RAs consist of spatially fed quasi-periodic reflective surfaces (QPRS) comprising hundreds or thousands of unit cells. Each unit cell is defined by a set of geometrical parameters that determine its design flexibility.

The distribution of the layout across the surface can be achieved by individually selecting unit cells capable of reflecting the local incident field to match a desired local aperture field phase, which is precomputed. This approach, known as phase-only synthesis, traditionally treats each cell as an ideal phase shifter, disregarding information about cell amplitude or cross components [1].

Alternatively, the cell distribution can be optimized globally by considering the full reflection matrix in both phase and amplitude. This approach, known as direct RA optimization, optimizes all unit cells simultaneously, focusing on achieving the desired scattered far-field, which is typically the ultimate goal of reflector design [2], [3], [4]. While the first approach is computationally efficient, it often leads to sub-optimal designs. The second approach, which yields more optimal far-field performance, is computationally more expensive because the cells in the layout need to be re-characterized or interpolated at each iteration [5].

Optimizing electrically large RAs typically involves a high number of degrees of freedom (d.o.f.). To handle the dimensionality and complexity of the problem, certain assumptions can be made. Firstly, the local periodicity assumption considers each cell as part of a periodic environment, avoiding the need for expensive simulations of the entire layout. This assumption implies that neighboring cells exhibit similar topology, ensuring layout continuity and smoothness, which are important design constraints [6], [7], [8].

One technique to reduce the dimensions of the optimization problem and improve the handling of optimization variables is to use continuous basis functions that depend on fewer d.o.f. to describe the geometries of the unit cells in the array. In previous works [9], [10], the geometrical variations of square patch elements were represented using continuous functions such as splines. However, this method failed to accurately represent the sharp geometrical variations occurring after a complete geometrical cycle. Instead, representing complex field quantities (aperture field) through continuous functions, while allowing each cell to be chosen individually to match the optimized field quantities, resolved this issue. However, this approach may result in abrupt layout variations [10].

Phoenix cells (PC), introduced in [11], possess the interesting property of rebirth capability. This means that the cell's geometry loops back to its initial configuration after completing a full phase cycle, without abrupt geometry variations. The order and type of the PC cycle can also be mixed [12]. This property has been effectively utilized in direct optimization processes for co-polarization [2], [13] and cross-polarization [14], [15] components using square or rectangular PCs, respectively. Exploiting the periodicity properties of PCs allows for the creation of phoenix cycle databases, enabling layout parametrization using continuous and derivable functions, without undesired sharp geometrical transitions.

For more details on the periodic features of Phoenix cycle databases, refer to the works [2], [13], [15], [14], [16], [17]. The database parametrization facilitates accurate interpolation of the database geometries, providing rapid access to the full reflection properties of any arbitrary geometry. This aspect is crucial for implementing a direct optimization process. Additionally, projecting the layout distribution onto a limited set of basis functions, such as splines, enables a reduced number of d.o.f. to describe the geometrical patterns of the RA, thereby reducing the dimensions of the direct optimization variables.

This paper aims to present the general principles of DOMES and its software modules (section II). It also covers the design and optimization of an electrically large deployable reflectarray composed of nine composite panels for S-band broadcast missions (section III). A modified optics and reduced-size engineering model is designed and optimized (section IV) and benchmarked against a theoretical equivalent aperture-shaped metallic reflector. Finally, conclusions are discussed in section V.

II. Direct optimization of RA

A. RA analysis tool

The primary modules of DOMES consist of an in-house software called Rivia, based on modified Physical Optics techniques and developed internally at Thales Alenia Space [18]. Rivia is a highly efficient and fully parallelized analysis program designed to handle the analysis of electrically large and complex radiating systems. It supports various types of surfaces, including metallic, dielectric, dichroic, and periodic surfaces such as frequency and polarization selective surfaces, for both reflection and transmission cases. Radiators can be positioned either in the near-field or far-field zone relative to each other.

Rivia allows for the comprehensive analysis of quasi-periodic surfaces, such as reflectarrays (RAs). It can handle the modeling of single or multi-panel RAs, as well as conformal RAs with arbitrary internal and external edges. This capability enables the consideration of complex mechanical inclusions, such as hinges, holes, or metal parts, in the radiation analysis.

Rivia also accounts for surface distortions caused by in-orbit thermoelastic effects. In particular, it allows the evaluation of their impact on the nominal radiation patterns. This feature is particularly useful when dealing with large physical apertures in space reflectors or RAs [15].

Within reflectarray analysis, design, and optimization, Rivia allows for the computation of various parameters, including the incident field, incidence angles, aperture field, scattered near-field and far-field patterns, and ideal reflection matrices. This last feature is performed by calculating the complex ratio of the incident field to the backscattered ideal aperture field when the desired far-field components are known.

Once the reflectarray model is constructed, Rivia allows the computation of the scattered far-field for the updated layout, which serves as the basis for evaluating the cost function in the optimization loop.

B. Unit cell characterization module and database construction

To ensure computational efficiency, the scattering behavior of the reflectarray is computed by assuming local periodicity. This means that each cell on the reflectarray surface is treated as if it is surrounded by identical cells. This assumption enables the characterization of the elementary cells within a periodic environment.

The industrial tool MIX, developed by Thales Alenia Space, is utilized as a module within DOMES to accurately predict the scattering behavior of the unit cells. MIX is a versatile program for analyzing periodic surfaces based on the Floquet expansion of the scattered field from the unit cell [19], [20]. It allows for the characterization of single or multiple grids, including capacitive grids (metallic patches on dielectric layers), inductive grids (holes on metallic sheets with or without dielectric support), or mixed grids (combinations of capacitive and inductive grids). This software provides accurate characterization of cells with complex geometric patterns, achieving high accuracy while requiring significantly lower computational effort compared to full-wave simulations.

The selection of unit cells for the reflectarray layout must satisfy two main constraints: achieving the desired phase delay in the local reflected field, which requires the ability to provide at least a complete (or nearly complete) 360° phase shift by varying the cell geometry, and maintaining a topology similar to that of the surrounding cells.

By combining different types and orders of Phoenix cells (PCs), it is possible to design a periodic Phoenix cycle in which the cell geometry returns to its initial state after a complete phase cycle. Previous works by the authors have presented examples of periodic and continuous databases composed of PCs [13], [14]. In this work, square PCs that can be deformed into rectangles are employed to exploit the asymmetry of the cell for dual circular polarization purposes [21]. The PC database, with a cylindrical mapping as described in [14], allows for fast access to the reflection matrices of the geometries during the optimization process.

C. Optimization problem formulation

The aim is to directly optimize the layout of the reflectarray by considering a cost function based on the amplitude distribution of the scattered far-field at a set of ground stations.

The *minimax* algorithm has proven to be one of the most suitable optimization algorithms for the direct optimization of shaped beam antennas [22], including recent developments for reflectarrays [2], [3], [5]. This algorithm works by minimizing the maximum loss for a worst-case scenario of a vectorial cost function with dimension l [23]. Defining the optimization variable state vector as $\mathbf{X} = \begin{bmatrix} X_1 & X_2 & ... & X_N \end{bmatrix}$, the cost function vector can be expressed as:

$$\mathbf{F^{obj}} = \begin{Bmatrix} f_1(X_1, ..., X_N) \\ f_2(X_1, ..., X_N) \\ f_3(X_1, ..., X_N) \\ ... \\ f_l(X_1, ..., X_N) \end{Bmatrix} \quad (1)$$

a) Optimization variables: In the formulation of the reflectarray optimization problem, the optimization variables correspond to the geometric parameters of each cell that compose the layout, denoted as $\mathbf{d}(x_{n,m}, y_{n,m})$. This implies that for an $N \times M$ reflectarray grid (cell grid) and i geometric parameters describing the cells $\begin{bmatrix} d_1 & d_2 & ... & d_i \end{bmatrix}$, the dimension of the variable space is given by:

$$N_{d.o.f.} = N \times M \times i. \quad (2)$$

For example, considering the cells described in a database like the one in [12], where the cell geometry is represented by the vector $\mathbf{d} = \begin{bmatrix} d_{1_x} & d_{1_y} & d_{2_x} & d_{2_y} \end{bmatrix}$, representing the horizontal and vertical dimensions of the slot and patches of the first and second order PC [12], the number of degrees of freedom would be $N_{d.o.f} = N \times M \times 4$. However, the cylindrical parametrization of the cell geometries [14] using variables ξ and h reduces the degrees of freedom to half, resulting in $N_{d.o.f} = N \times M \times 2$.

Another advantage of cell parametrization is the ability to describe the reflectarray layout using continuous functions, such as tensorial bi-cubic splines, to represent the database through continuous and differentiable functions. The optimization variables can be redefined based on the following considerations: given an initial surface distribution of the parameters $\xi(x_{n,m}, y_{n,m})$ and $h(x_{n,m}, y_{n,m})$, the optimization variables are defined by tensors of spline coefficients $\Delta\Xi_{k_x,k_y}$ and $\Delta H_{k_x,k_y}$, which represent variations with respect to an initial parameter distribution $\xi_{initial}(x_{n,m}, y_{n,m})$ and $h_{initial}(x_{n,m}, y_{n,m})$. This can be expressed as:

$$\xi(x_{n,m}, y_{n,m}) = \xi_{initial}(x_{n,m}, y_{n,m}) + c_{n,m_{k_x}} \Delta\Xi_{k_x,k_y} c_{n,m_{k_y}} \quad (3)$$

$$h(x_{n,m}, y_{n,m}) = h_{initial}(x_{n,m}, y_{n,m}) + c_{n,m_{k_x}} \Delta H_{k_x,k_y} c_{n,m_{k_y}} \quad (4)$$

This representation offers two main advantages: the spline description of the variation function ensures continuity and differentiability of the parametric surface at each iteration, guaranteeing layout smoothness. Additionally, it significantly reduces the number of degrees of freedom in the optimization problem. Considering the dimensions of the matrices, where $N \times M$ represents the size of the reflectarray grid and $K_x \times K_y$ denotes the size of the $k_x - k_y$ grid, the tensors involved in the spline representation of the unwrapped surface have dimensions $\Delta\Xi_{k_x,k_y}((K_x+k-2)\times(K_y+k-2))$, $c_{n,m_{k_x}}(N \times (K_x + k - 2))$, $\Delta H_{k_x,k_y}((K_x + k - 2) \times (K_y + k - 2))$, and $c_{n,m_{k_x}}(N \times (K_x + k - 2))$, $c_{n,m_{k_x}}((K_y + k - 2) \times M)$. Here, k represents the multiplicity of knots on the knot grid domain borders, with $k = 4$ for bi-cubic splines. The number of degrees of freedom depends on the number of spline knots considered and can be expressed as:

$$N_{d.o.f} = (K_x + k - 2) \times (K_y + k - 2) \times 2 \quad (5)$$

In general, a small number of knots is sufficient to accurately describe the parametrized surface of the reflectarray, with $K_{x,y} \ll M, N$. The optimization variables are directly linked to the cell geometry $\mathbf{d}(x_{n,m}, y_{n,m})$ at an incidence $(\theta^{inc}n, m, \phi^{inc}n, m)$, identified by the reflection matrix $\Gamma(\theta^{inc}_{n,m}, \phi^{inc}_{n,m}, f)$. This allows for rapid access to the scattering matrix of an arbitrary cell by interpolating the phase and amplitude of each reflection matrix component in the database using local cubic functions. Local cubic interpolation of scattering coefficients provides accurate cell characterization with low computational effort [14], [5].

b) Cost function: The cost function is defined based on the objectives of the direct optimization, which involves reducing the error with respect to a target radiation pattern or mask. The cost function aims to minimize the maximum residuals between the radiation pattern computed at a set of ground stations defined in u_{sta}, v_{sta} coordinates and a goal defining the desired amplitude of the radiated field components. For instance, if the goal is to optimize the co-polarization and cross-polarization far-field components at a given frequency, the cost function can be expressed as:

$$\mathbf{F^{obj}} = \begin{Bmatrix} max(0, G_{CO/XPD_{goal}}(u_1, v_1) - G_{CO/XPD}(u_1, v_1)) \\ max(0, G_{CO/XPD_{goal}}(u_2, v_1) - G_{CO/XPD}(u_2, v_1)) \\ ... \\ max(0, G_{CO/XPD_{goal}}(u_{st}, v_1) - G_{CO/XPD}(u_{st}, v_1)) \\ max(0, G_{CO/XPD_{goal}}(u_1, v_2) - G_{CO/XPD}(u_1, v_2)) \\ ... \\ ... \\ max(0, G_{CO/XPD_{goal}}(u_{st}, v_{st}) - G_{CO/XPD}(u_{st}, v_{st})) \end{Bmatrix} \quad (6)$$

If multiple frequencies are considered, the dimension of the cost function vector would increase accordingly. The evaluation of the cost function can be performed using the in-house physical optics software Rivia (section II-A).

III. Large Deployable RA for Direct Broadcast Satellite in S-band

We present an application example of an electrically large reflectarray (RA) designed for contour beam applications. Specifically, we consider a 7m S-band deployable RA. In the context of high-gain contour beam antennas, single-feed RAs can offer competitive performance and manufacturing cost advantages over single-feed mesh reflectors. High surface shaping levels in mesh reflectors are a challenging task, and the need for large-scale manual assembly makes them expensive solutions [24]. Here, we provide a summary of the RA configuration, mission specifications, and performance evaluation within a 1% fractional bandwidth. We compare the performance against a reference shaped reflector and a conventional phase-only (PO) synthesis approach. For more

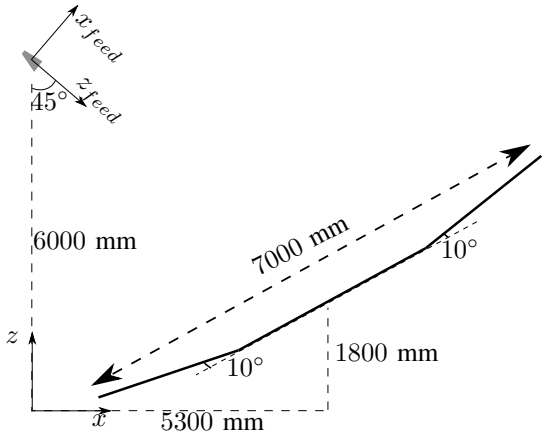

Fig. 1: Side view of the RA geometry.

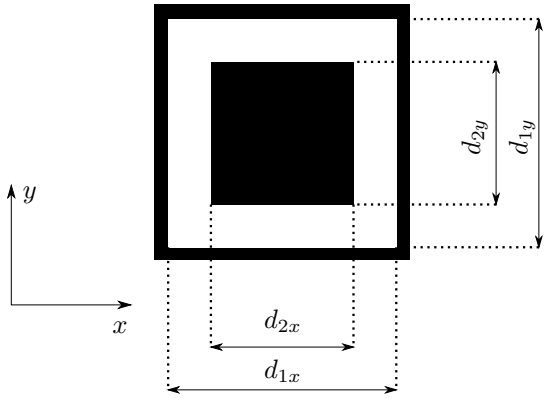

Fig. 2: Unit cell geometry.

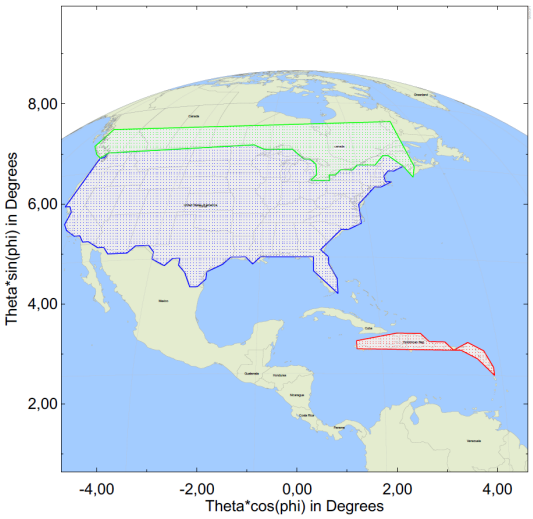

Fig. 3: Coverage regions of the mission.

details on the large deployable RA design process, please refer to [16].

A. Deployable RA Architecture and Requirements

The deployable RA architecture consists of nine planar panels and incorporates a system of high-precision hinges for deployment. Its deployment scheme is similar to that of a conventional reflector with similar building blocks. Figure 1 shows a side view of the RA in its deployed configuration. The key features of the RA are summarized in Table I.

TABLE I: RA features

RA geometry	circular
Number of flat panels	9
Physical aperture	$D = 7000\,m$
Focal distance	6000 mm
Aperture center	5300 mm
Offset angle	45°
Clearance	1800 mm

The RA employs rectangular slot/patch combination elements described in [14], [16] as the array elements. Figure 2 illustrates the geometric degrees of freedom (d.o.f.) of the unit cell, which are the slot/patch dimensions $d_{1x,y}$ and $d_{2x,y}$. The nine-panel RA comprises a total of 22,434 actual array elements, resulting in 89,736 optimization variables. However, this number is reduced to two through an efficient database parameterization technique described in [14].

A use-case coverage region is defined to evaluate the RA's performance. The selected target covers three regions: the Continental United States (CONUS), Canada, and the Caribbean area (see Figure 3 and Table II). Additionally, strict requirements for specific cities are specified. The coverage region is relatively large in the East-West dimension (approximately 8°) but restricted in the North-South dimension (approximately 4°).

The preliminary layout is obtained through phase-only synthesis, where the ideal phase law is derived from the backscattering of a far-field obtained from a previously optimized theoretical shaped reflector with the same physical aperture.

The optimization problem aims to find the optimal distribution of parameters describing the cell geometries that best satisfy the optimization goals for the co-polarization and cross-polarization components at a single central frequency.

B. Optimized RA Performance

Details of the optimized RA layout in terms of parametric surfaces are provided in [16]. The layout exhibits continuity and avoids abrupt geometric variations, as shown in Figure 4.

Figure 6 presents contour plots of the co-polarization and cross-polarization radiated by the optimized RA at the central frequency for the LHCP component. The RHCP component exhibits a similar behavior, which is not included in this paper for brevity. The requirements are met within the coverage regions, even considering an additional 1 dB of uncertainty margin. Table III compares the performances of the optimized RA (referred to as RA DO), the initial layout obtained through phase-only synthesis of an ideal phase law derived from a reference metallic reflector (referred to as RA PO), and the

TABLE II: Target Mission

Orbit/mission	Geostationary/broadcast satellite
Polarization	Double circular *RHCP-LHCP*
Bandwidth	$\approx 1\%$ S-band
Central frequency	$f_0 = 2330$ MHz

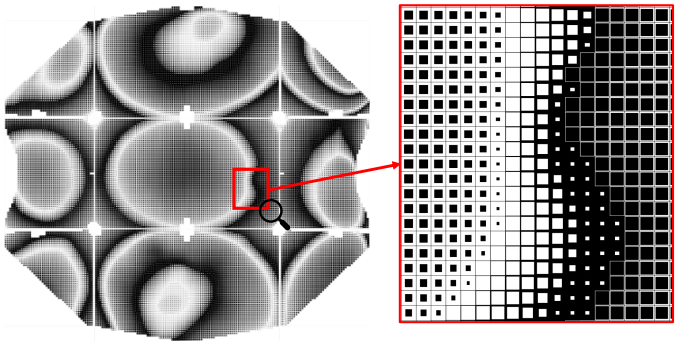

Fig. 4: Layout issued from direct optimization [16].

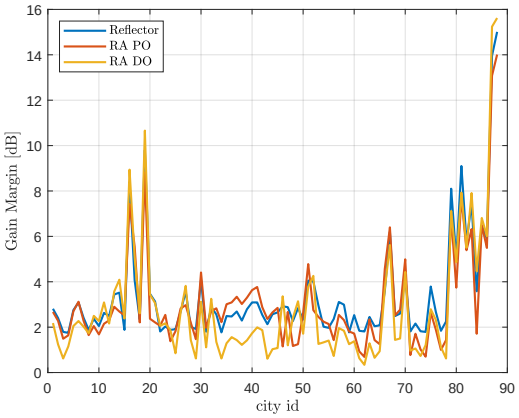

Fig. 5: Gain margins for the LHCP component on the main cities [16].

reference metallic reflector's performances. The optimized RA outperforms the initial layout in terms of minimum gain in the coverage regions. Importantly, the optimized RA exhibits improved cross-polarization discrimination in both polarizations, meeting the requirements. It should be noted that while the optimized RA better satisfies the gain margins for coverage regions, it is slightly penalized when compared to the reflector and initial layout in terms of co-polarization gain margins for a large set of cities (see Figure 5). Only LHCP is presented since for the RHCP very similar results are obtained.

The current results are shown for a 1% bandwidth since the optimization was performed at the central frequency. The PC features and the faceted configuration ensure compliance with the gain margin requirements for at least a 10% bandwidth. Performance degradation of the current layout occurs at a 20% bandwidth on the frontiers of the coverage regions, while gain margins are still respected for the main cities. An optimization considering a broader frequency band could further enhance the performances within the bandwidth. Additional details will be presented during the conference.

C. Thermoelastic distortion impact on the radiation pattern

The mechanical team conducted surveys to evaluate the impact of thermal gradients in orbit on the RA panels deformations due to their large dimensions. They supplied structural displacement data in order to evaluate the impact of such deformations on the RA performance. The analyses were carried out at the central frequency for both circular polarizations. Seven different load cases deformation outputs were analyzed in terms of co-polarization and cross-polarization degradation.

In terms of the minimum gain, the worst-case scenario exhibited similar degradation for both polarizations. The loss reached up to 0.7 dB in RHCP for a particular city, which remains within compliance limits considering the gain margin obtained from the direct optimization (DO) process.

IV. RA Engineering Model

In order to facilitate the manufacturing and testing process of the large dimensions (7m aperture) RA, a reduced-size engineering model (EM) was developed. The EM consists of two out of the nine panels of the RA, with modified optics. This allows it to fit into the near-field test range (NFTR) located in Thales Alenia Space facilities in Toulouse. The primary objectives of the EM are to validate the design and technological processes of the large deployable RA for future product deployment. The following section provides an overview of the EM's features.

A. EM Architecture and Requirements

The EM comprises two panels with modified optics, as shown in Figure 7. This necessitates a new RF layout design and optimization from scratch. The relative inclination between the two panels is maintained, as well as the focal distance. The panels are separated by a gap of 10mm, with 5mm coplanar alignment for each panel. The offset distance has been reduced from 5300 mm to 3100 mm, resulting in a corresponding decrease in the offset angle. The same feed used for the nine-panel RA is retained, but to achieve an almost uniform taper at the panel borders, the feed is directed towards the junction between the two panels, introducing two additional consecutive feed reference frame rotations.

The two selected reflective surfaces (Figure 8a) consist of a total of $88 \times 52 \times 2$ cells, with approximately 2.5% of the active physical aperture being occupied by mechanical inclusions (such as hinges and HRM) shown in Figure 8b. The mechanical inclusions are considered as short-circuited cells in the model, and their detrimental effects are taken into account and compensated for at the global level through the direct optimization process.

The selected coverage region for the EM corresponds to the CONUS region, as defined in Section III-A, without specific city requirements. Therefore, the design and optimization

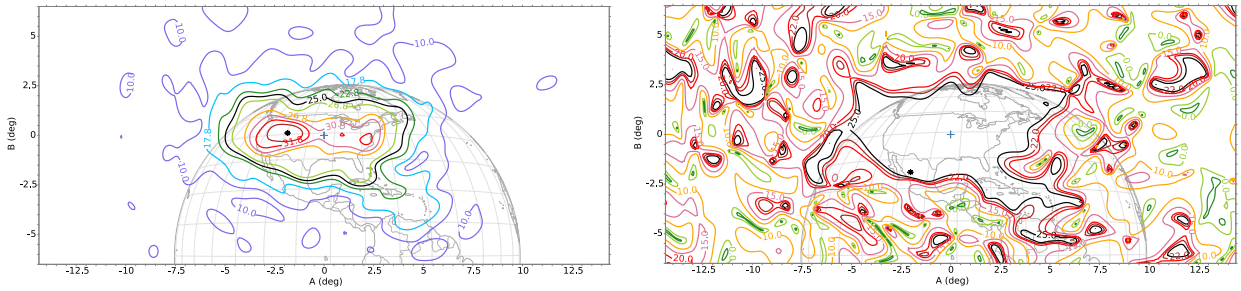

(a) co-polarization, LHCP component.

(b) XPD, LHCP component.

Fig. 6: Optimized RA radiation pattern at center frequency f_0.

TABLE III: RAs and reference reflector performances comparison in the frequency band in the three targeted coverage regions.

Coverage	**CONUS**						**Canada**						**Caribbean**					
Goal	$G_{min} = 25$ dB			$XPD_{min} = 25$ dB			$G_{min} = 22$ dB			$XPD_{min} = 25$ dB			$G_{min} = 16$ dB			$XPD_{min} = 22$ dB		
f	f_-	f_0	f_+	f_-	f_0	f_+	f_-	f_0	f_+	f_-	f_0	f_+	f_-	f_0	f_+	f_-	f_0	f_+
LHCP																		
Reflector	25.8	25.7	25.7	26.8	27.1	28.4	20.9	20.9	20.8	28.1	28.6	28.9	16.7	16.8	16.9	23.7	23.9	24.9
RA PO	24.7	24.6	24.5	20.7	20.7	21.1	20.8	20.2	19.7	21.1	21.3	21.7	14.6	14.2	13.6	11.9	11.4	11.0
RA DO	26.3	26.3	26.2	27.1	27.0	27.2	22.5	22.3	22.5	26.3	27.0	26.9	17.2	17.8	17.7	23.7	23.9	23.8
RHCP																		
Reflector	24.5	24.5	24.4	28.3	28.3	28.9	22.9	22.8	22.7	28.1	28.2	29.2	16.7	16.7	16.9	19.1	19.4	20.5
RA PO	23.4	23.3	23.2	22.0	21.9	22.0	22.1	22.1	22.1	22.6	22.4	22.3	12.5	11.9	11.2	19.5	19.3	19.3
RA DO	26.1	26.2	26.0	26.7	27.0	27.0	23.59	23.45	23.58	27.1	27.0	26.7	17.6	17.3	16.9	23.3	23.6	23.7

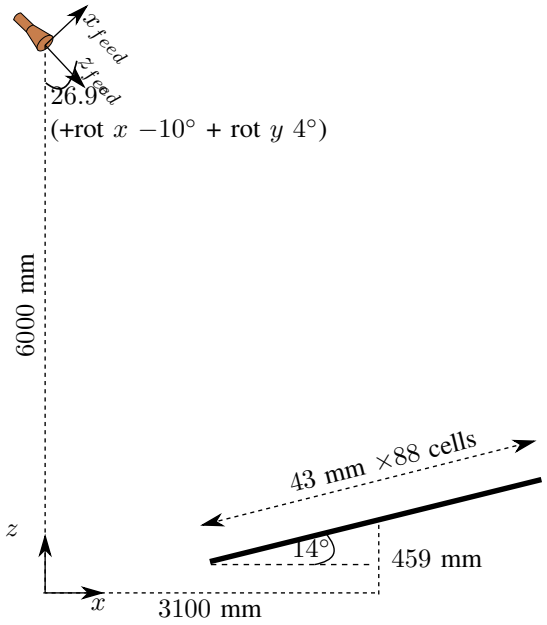

Fig. 7: Side view of the EM geometry.

requirements for the EM are less stringent compared to the full-size RA.

B. EM Design and Optimization

For the EM design and optimization, the same unit cell geometry and methodology presented in Section III are employed. The properties of the dielectric substrate and honeycomb structure have been updated with experimental data provided by ESA. Similar to the 7m aperture RA, a reference shaped reflector with the same optics and feed, optimized using Ticra POS, was utilized for performance benchmarking.

Figure 8c illustrates the layout of the optimized EM. The resulting radiation pattern footprint on Earth in terms of co-polarization and XPD is shown in Figure 9. Table IV provides the performances in a 1% bandwidth, as well as in a 10% bandwidth. In the latter case, LHCP and RHCP Gaussian feed illumination was used for the reflector, RA PO, and RA DO, as the supplied real feed was optimized for a 1% bandwidth and not suitable for a larger bandwidth.

The direct optimization process was performed at three frequencies within a 1% bandwidth, resulting in far-field performances that comply with the specifications. The minimum gain margin achieved was 1.6 dB, and the minimum XPD margin was 0.9 dB within the 1% bandwidth. Verification in a 10% bandwidth also demonstrated performances that met the specifications, with a minimum gain margin of 0.9 dB. Although the optimization could have been conducted in a 10% or larger bandwidth, the actual optimization was limited to a 1% bandwidth due to the feed's design specifications. An EM direct optimization in a 20% bandwidth using a Gaussian feed was successfully performed and will be presented at the conference.

Comparing the optimized RA with the reference shaped reflector and the RA PO, the optimized EM exhibits superior performances in terms of minimum gain and XPD within the coverage region. This can be attributed to the RA optimization process incorporating more optimization parameters compared to the shaped reflector. While the shaped reflector is optimized

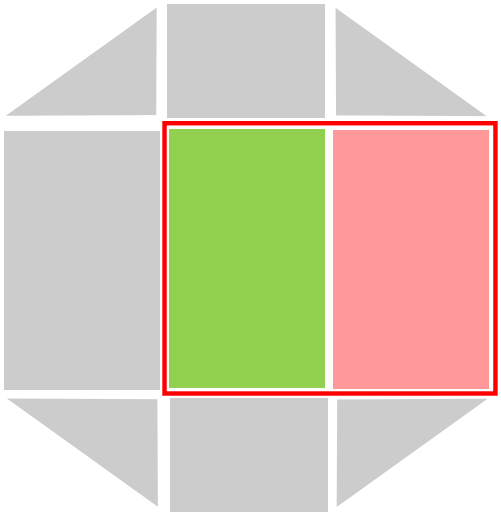

(a) Portion of the nine-panel RA considered for the EM.

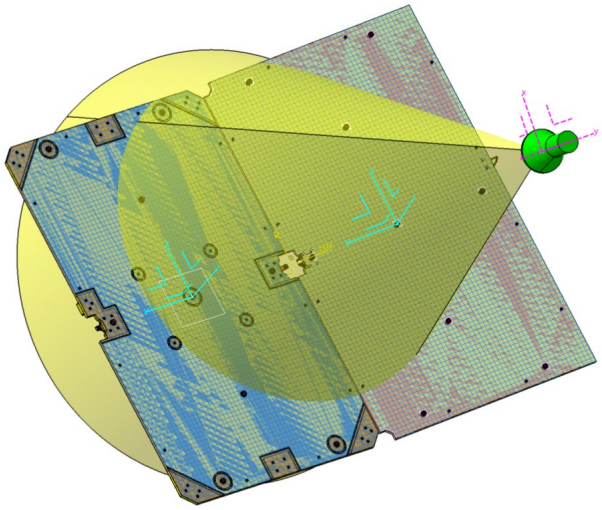

(b) Two-panel EM with mechanical inclusions and new external edges visible. Highlight on feed re-pointing at panels junction with ray tracing.

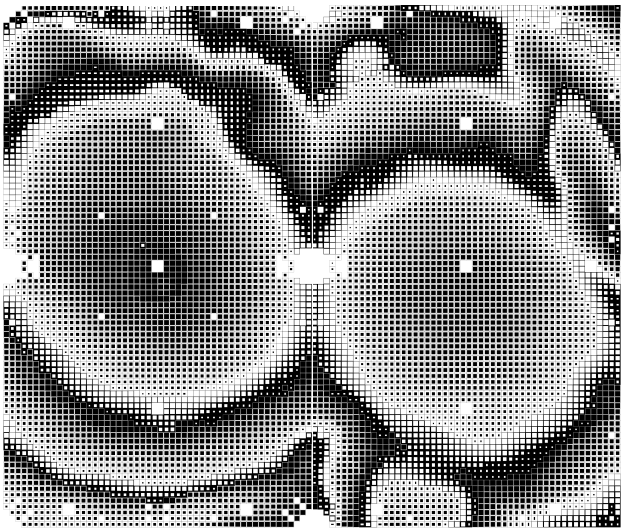

(c) EM layout derived from direct optimization with mechanical inclusions represented as holes.

Fig. 8: Engineering model RA.

only on the coefficients of spline functions representing the surface shape, the RA optimization encompasses the coefficients of spline functions representing the cell index in the database, directly linked to the phase law (gain specifications), as well as the spline functions representing the cells' distortion index (transforming squares into rectangles to comply with XPD specifications). Furthermore, the low amplitude taper of the incident field, which results in high spill-over losses (around 2.29 dB for the reference reflector and 2.35 dB for the RA with mechanical inclusions and holes), does not allow for effective optimization with a single degree of freedom (metallic surface shape). Such conditions are not suitable for reflector shaping optimization protocols. Despite this, the reference reflector and RA performances presented in Section III are comparable. This use case highlights the potential of the presented research software tool, which can be customized for specific non-canonical applications.

C. Optimization Process Interpolation Accuracy Considerations

The optimization process requires fast access to the full reflection properties of each unit cell (including direct and crossed reflection coefficients in amplitude and phase) at its incident angle as seen from the feed. Given the high number of unit cells in the RA layout, interpolation on incidences and database cell geometries is necessary. In this section, we verify the accuracy of the interpolation by comparing the radiation

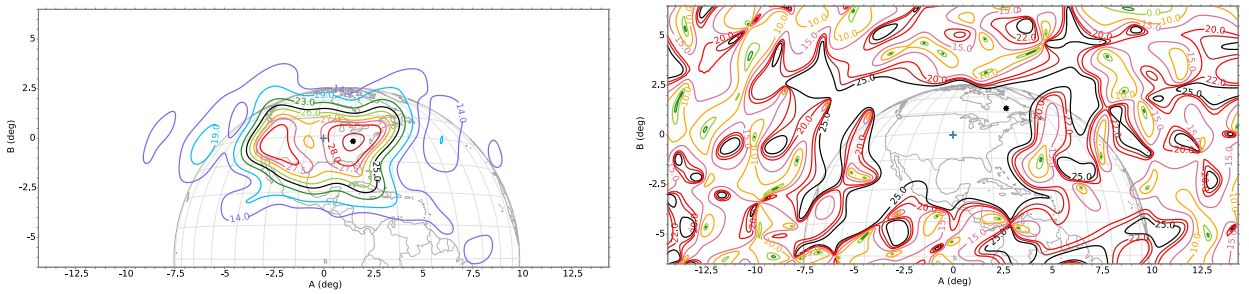

(a) co-polarization, LHCP component.

(b) XPD, LHCP component.

Fig. 9: Optimized EM RA radiation pattern at center frequency f_0.

TABLE IV: EM RAs and reference reflector performances comparison in a 10% frequency band on CONUS coverage region. Gaussian feed is considered for the edge frequencies il the 10% BW.

Coverage	**CONUS**									
Goal	$G_{min} = 25$ dB					$XPD_{min} = 25$ dB				
f	$f_0 - 5\%$ Gauss. feed	$f_0 - 0.5\%$	f_0	$f_0 + 0.5\%$	$f_0 + 5\%$ Gauss. feed	$f_0 - 5\%$ Gauss. feed	$f_0 - 0.5\%$	f_0	$f_0 + 0.5\%$	$f_0 + 5\%$ Gauss. feed
					LHCP					
Reflector	22.7	22.5	22.7	22.5	23.2	44.0	26.5	26.2	24.6	43.5
RA PO	21.6	22.2	22.2	22.2	23.3	28.5	25.2	23.9	21.9	25.0
RA DO	26.0	26.6	26.6	26.6	27.0	27.7	26.8	27.2	25.9	26.5
					RHCP					
Reflector	22.1	21.8	21.8	21.83	22.5	43.6	23.7	24.5	24.3	43.2
RA PO	20.7	21.3	21.3	21.3	22.2	30.	23.7	25.3	25.0	29.6
RA DO	25.9	26.6	26.8	26.8	26.8	28.6	28.8	28.4	27.0	26.0

pattern of a layout using interpolated unit cell reflection coefficients with that of a layout computed by characterizing each unit cell individually. The considered incidence angles samples are $\theta^{inc} = 0° : 5° : 40°$ and $\phi^{inc} = 0° : 15° : 90°$, resulting in a total of 63 incidence samples. The database contains 85 rectangular PC geometries. The interpolation process involves two steps: bilinear interpolation on the incidence angles, followed by local bi-cubic interpolation of the cylindrical database [14] on the geometries. Figure 10 shows a superposition of the radiation patterns obtained from the optimization process and the layout characterized unit cell by unit cell. The correlation between the two cases demonstrates the effectiveness of the interpolation method and confirms the accuracy of the cost function evaluation for gain and XPD during the optimization process.

V. Conclusions

This paper introduces a highly efficient multi-modular tool, DOMES, for the analysis, design, and optimization of RA antennas. DOMES consists of two main modules: Rivia, a physical optics tool for large aperture and multi-scatterers analysis, and MIX, a fast and efficient periodic surfaces analysis tool. These modules are integrated within DOMES using a parametrization and interpolation process that leverages the properties of periodic cells. The software tool is flexible and can be customized for various quasi-periodic surface applications. Two applications related to electrically large RA antennas are presented. The first application focuses on a large deployable faceted RA composed of nine composite panels. The optimization process resulted in improved performances compared to classical synthesis methods (such as phase-only synthesis) and demonstrated competitive performances comparable to an equivalent aperture theoretical shaped reflector. The second application involves the design and optimization of an engineering model (EM) consisting of two out of the nine panels of the large deployable reflectarray. The direct optimization process achieved improved performances compared to a theoretical shaped reflector, with gains up to 2 dB within the coverage region. The interpolation parametrization and interpolation process were verified to be highly effective in terms of accuracy. In both applications, Rivia enabled the modeling of mechanical inclusions, which were taken into account during the RA optimization process. Additionally, useful functionalities, such as evaluating the impact of in-orbit thermo-elastic distortions, were demonstrated for the nine-panel RA. Overall, the presented research software tool exhibits great potential for customization to specific non-canonical use cases. The software modules are in continuous evolution, on one hand, to improve the computational efficiency of the optimization program, on the other hand, to be adapted for future electrically large aperture antenna concepts.

Acknowledgements

This work was supported in part by the European Commission through the H2020 Project REVOLVE under Grant MSCA-ITN2016-722840 and in part by the French Ministry of Higher Education, Research and Innovation through the “France Relance” project SOAR under Grant ANR-21-PRRD-

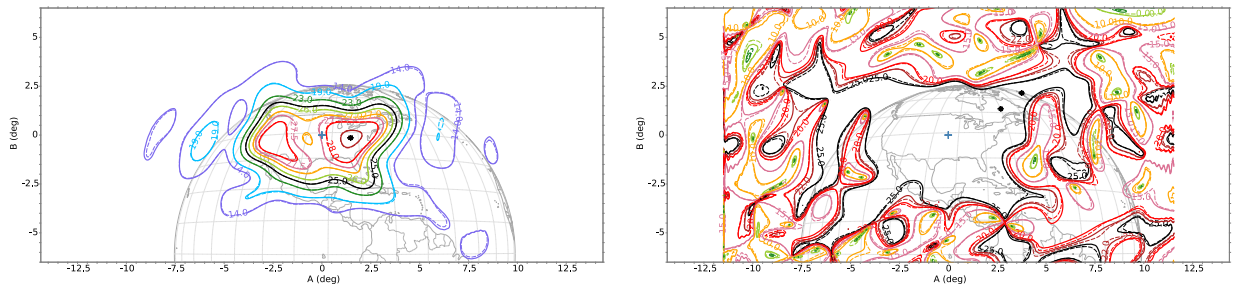

(a) Co-polarization, LHCP component.

(b) XPD, LHCP component.

Fig. 10: Radiation pattern at the center frequency f_0. Continuous lines layout characterized unit cell by unit cell, dashed lines interpolated layout.

0037-01. The development of the S-band RA product isrealized thanks to the support of Luxembourg Space Agency (LSA) & EURO-COMPOSITES S.A and supervised by the European Space Agency. The authors would like to thank R. Chiniard, E. Labiole, C. Leclerc, O. Bardel, and J.-A. Duran-Venegas for supplying the use case and fundamental data.

REFERENCES

[1] J. A. Zornoza and J. A. Encinar. Efficient phase-only synthesis of contoured-beam patterns for very large reflectarrays. *Int. J. of RF and Micro. Comput.-Aided Eng.*, 14(5):415–423, 2004.

[2] V. Richard, R. Loison, R. Gillard, H. Legay, M. Romier, J.-P. Martinaud, D. Bresciani, and F. Delepaux. Spherical mapping of the second-order phoenix cell for unbounded direct reflectarray copolar optimization. *Prog. In Electromagn. Res. C*, 90:109–124, 2019.

[3] M. Zhou, S. B. Sørensen, Oleksiy S. Kim, E. Jørgensen, P. Meincke, and O. Breinbjerg. Direct optimization of printed reflectarrays for contoured beam satellite antenna applications. *IEEE Trans. on Antennas and Propag.*, 61(4):1995–2004, 2013.

[4] D. R. Prado, M. Arrebola, M. R. Pino, and G. Goussetis. Contoured-beam dual-band dual-linear polarized reflectarray design using a multiobjective multistage optimization. *IEEE Trans. on Antennas and Propag.*, 68(11):7682–7687, 2020.

[5] M. Zhou, S. B. Sørensen, Oleksiy S. Kim, E. Jørgensen, P. Meincke, O. Breinbjerg, and G. Toso. The generalized direct optimization technique for printed reflectarrays. *IEEE Trans. on Antennas and Propag.*, 62(4):1690–1700, 2014.

[6] M.-A. Milon, R. Gillard, D. Cadoret, and H. Legay. Analysis of mutual coupling for the simulation of reflectarrays radiating cells. In *First Eu. Conf. on Antennas and Propag. (EUCAP 2006)*, pages 1–6, 2006.

[7] M.-A. Milon, R. Gillard, and H. Legay. Rigorous analysis of the reflectarray radiating elements: Characterisation of the specular reflection effect and the mutual coupling effect. In *29th ESA Antenna Workshop on Multiple Beams and Reconfigurable Antennas*, 2007.

[8] H. Legay, D. Bresciani, E. Labiole, R. Chiniard, and R. Gillard. A multi facets composite panel reflectarray antenna for a space contoured beam antenna in ku band. *Prog. In Electromagn. Res. B*, 54:1–26, 2013.

[9] M. Zhou, S. B. Sørensen, E. Jørgensen, and P. Meincke. Efficient optimization of large reflectarrays using continuous functions. In *2013 7th Eur. Conf. on Antennas and Propag. (EuCAP)*, pages 2952–2956, 2013.

[10] M. Zhou, S. B Sørensen, P Meincke, E Jørgensen, Oleksiy S Kim, O. Breinbjerg, and G. Toso. An accurate and efficient design tool for large contoured beam reflectarrays. In *ESA Workshop on Large Deployable Antennas, Noordwijk, Netherlands*, 2012.

[11] L. Moustafa, R. Gillard, F. Peris, R. Loison, H. Legay, and E. Girard. The phoenix cell: A new reflectarray cell with large bandwidth and rebirth capabilities. *IEEE Antennas and Wireless Propagation Letters*, 10:71–74, 2011.

[12] A. Guarriello, G. Courtin, R. Loison, and R. Gillard. A general equivalent circuit model for phoenix cells. *IEEE Trans. on Antennas and Propag.*, 69(11):7982–7986, 2021.

[13] V. Richard, R. Gillard, R. Loison, H. Legay, M. Romier, J.-P. Martinaud, D. Bresciani, and F. Delepaux. Advanced synthesis of reflectarrays using a spherical mapping of the 2nd order phoenix cell. In *2019 13th Eur. Conf. on Antennas and Propag. (EuCAP)*, pages 1–5, 2019.

[14] A. Guarriello, R. Loison, D. Bresciani, H. Legay, and G. Goussetis. Continuous rectangular phoenix cells mapping for direct copolar and crosspolar optimization of quasi-periodic reflective surfaces. In *2023 17th Eur. Conf. on Antennas and Propag. (EuCAP)*, pages 1–5, 2023.

[15] A. Guarriello, R. Loison, D. Bresciani, H. Legay, and G. Goussetis. Structural and radio frequency co-design and optimization of large deployable reflectarrays for space missions. *IEEE Trans. on Antennas and Propag.*, 71(5):3916–3927, 2023.

[16] A. Guarriello, D. Bresciani, R. Loison, J.-A. Duran-Venegas, E. Labiole, C. Leclerc, R. Chiniard, and O. Bardel. Design and optimization of a double circular polarization large deployable reflectarray for direct broadcast satellite in s-band. In *2023 17th Eur. Conf. on Antennas and Propag. (EuCAP)*, pages 1–5, 2023.

[17] A. Guarriello, R. Loison, D. Bresciani, H. Legay, and G. Goussetis. Advanced optimization of an isoflux reflectarray. In *2022 IEEE MTT-S Int. Conf. on Numer. Electromagn. and Multiphys. Model. and Optim. (NEMO)*, pages 1–4, 2022.

[18] D. Bresciani and S. Contu. Scattering analysis of dichroic subreflectors. *Electromagn.*, 5(4):375–407, 1985.

[19] D. Bresciani. A unified approach to the characterization of frequency and polarization selective surfaces. In *Proc. of IEEE Antennas and Propag. Soc. Int. Symp.*, pages 1960–1963 vol.3, 1993.

[20] S. Contu and R. Tascone. Scattering from passive arrays in plane stratified regions. *Electromagn.*, 5(4):285–306, 1985.

[21] D. Bresciani, H. Legay, E. Labiole, and G. Caille. Antenne réseau réflecteur à compensation de polarisation croisée et procédé de réalisation d'une telle antenne. *Patent FR2957719*, 2011.

[22] C. Klein. Design of shaped-beam antennas through minimax gain optimization. *IEEE Trans. on Antennas and Propag.*, 32(9):963–968, 1984.

[23] The Mathworks, Inc., Natick, Massachusetts. *Optimization Toolbox Version 8.2 (MATLAB v. 9.5 R2018b)*, 2018.

[24] Y. Zhang, B. Dong, G. Yang, D. Yang, and S. Zhang. Design technique for a shaped-reflector antenna with a three-layer cable net structure. *IEEE Trans. on Antennas and Propag.*, 69(1):109–121, 2021.